Silicon (2023) 15:1381–1391
https://doi.org/10.1007/s12633-022-02105-8

ORIGINAL PAPER

SoI Based Optical 1 × 2 Wavelength Independent 3-dB Power Splitter Design Using Three Rectangular Cross-Sectional Cuboidal Waveguides

Devansh Srivastava[1] · **Shalini Vardhan**[2] · **Ritu Raj Singh**[2]

Received: 3 June 2022 / Accepted: 2 September 2022 / Published online: 19 September 2022

Abstract
Silicon-on-Insulator (SoI) based 1 × 2 3-dB wavelength independent optical power splitter is designed which consist of three parallel cuboidal waveguides of rectangular cross-sectional area. Input power, that is to be split, is injected at the central cuboid, also called primary waveguide. Split output taken from the ports defined at the other end of secondary cuboids, known as secondary waveguides. Output power in each secondary waveguide, is nearly 45% of the total injected power. A theoretical model is built to investigate the normalized power flux in primary and secondary waveguides mathematically. The theoretical model is justified by the achieved simulation results using Finite Element Method (FEM). The width of the rectangular cross-section of primary and secondary waveguide is optimized, considering confinement factor and mode effective area. This is followed by optimization of the gap between primary and secondary cuboidal waveguides and evaluation of optimum longitudinal length of primary waveguide for 3 dB splitting application. The proposed design for 3 dB splitting is wavelength independent which is a valuable property for optical devices. Moreover, the design excludes any bending or tampering of the cuboidal waveguides, thereby avoiding any scope of bending loss. This, consequently, reduces the net loss associated with the splitter design.

Keywords Silicon photonics · Integrated photonic · Optical waveguides · Silicon-on-insulator waveguides · Beam splitter · Directional coupler

1 Introduction

Optical splitters are an important component of optical communication. Numerous optical instruments such as optical switches, modulators, multiplexers, optical phased arrays sensing, pharmacology, etc.; [1–8] use such power splitters. These are countless applications of the optical power splitter. The primary objective of these splitters is to distribute the power evenly among the waveguides in a pre-defined ratio [9]. In the case of a 3-dB splitter, the ratio is taken as 1:1. Researchers had worked intensively on constructing an optimized low-loss [10], ultra-high bandwidth [11, 12] and polarization insensitive [13] power splitters. Several methods of design were proposed to achieve the above mentioned characteristics [14–16].

In 1999, *Neil* et al made an analysis on Mach-Zehnder Interferometer (MZI) for power splitting and optical switching. In this work, generalized MZI was employed and both phase deviation and optical power splitting ratio deviation was studied [17]. Earlier, Multi-Mode Interference (MMI) based optical splitters were rapidly gaining popularity [18–20]. In 2001, *Hongzhen Wei* et al proposed a compact ultra-band 3-dB MMI based coupler in SoI [18] with length as small as *398 μm* and an excess loss of *9.9 dB*. Following this, in 2004, *Frandsen* et al introduced a photonic crystal waveguide for optical splitting [21]. The team proposed a planar photonic waveguide Y splitter for ultra-low loss 3 dB splitting of TE polarized light with a minor excess loss of 1-2 dB [22]. In the same year, *Sangin Kim* et al proposed a photonic crystal-based 3 dB splitter-combiner [23]. The work on power splitter was extended by the team of *Quan Xu* in which a coupled-cavity waveguide-based splitter was proposed. This

✉ Ritu Raj Singh
rituraj.singh@nsut.ac.in

[1] Department of Electronics and Communication Engineering, Indian Institute of Information Technology Ranchi, Ranchi, Jharkhand, India

[2] Department of Electronics and Communication Engineering, Netaji Subhash University of Technology, New Delhi, India

design gave promising results and transmitted up to 47.5% power. Furthermore, *Shaohua Tao* et al designed an optical splitter with variable splitting ratio [24]. The design witnessed a minor coupling loss of *2.6 dB/coupling* and was compact in size. *Xun Chen* et al proposed another silicon-bent directional coupler based broadband power splitter [25]. The design exhibited a minimal excess loss of less than *1 dB* and a very compact size of *50* μm.

In above-mentioned methods of design, the waveguides were excited with even and odd modes initially and these modes interacted with each other. However, *Han Yun* et al suggested a 2×2 adiabatic 3 dB coupler on SoI rib waveguides [26]. Unlike other designs, in adiabatic coupler, either of the mode was excited in the waveguide. This proposed adiabatic splitter gave 49.6%–50.4% of power transmission, which was a promising result for 3 dB splitting. In 2016, *Yang Wang* et al proposed another adiabatic tapered silicon waveguide-based power splitter [11]. The splitter exhibited excess loss of *0.19* dB for TE mode and *0.14* dB for TM mode. Owing to extensive and long-time research on splitters, the power splitters had come a long way.

The primary objective of this paper is to introduce a SoI based wavelength-independent 2×1 3 dB power splitter without introducing any bending or tapering. The paper begins with introduction, followed by design and theory of the waveguide. Then the width of the rectangular waveguides is optimized. Further, the gap between the primary and secondary waveguide is optimized.

The novelty of the design comes from the fact that optical power splitting is done using three cuboidal straight tampering-less waveguides. The structure of the proposed broad-band 3 dB splitter does not consist of any bending, thereby inhibiting any scope of bending loss. In this manuscript, the concept of intra-modal coupling between primary and secondary waveguides, for the exchange of optical power, is utilized in such a way that the losses associated with tampering, bending, and reforming of the waveguide can be avoided. When the optical power is injected in the primary waveguide, it is split equally into two secondary waveguides. This split optical power in their respective secondary waveguides have been restricted to couple back to the primary waveguide by intentionally choosing the length of the primary waveguide. The length of the primary waveguide is chosen in kind that the 3 dB split power remains in the secondary waveguide and thus can be extracted from the output ports. In other publications, similar methodology has been adopted, but with difference in design structure. In 2015, *Hseng-Tsong Wang* et al came up with a 3 dB splitter design in which the paper considered a straight primary waveguide and bent secondary waveguides for the application of power splitting [27]. This design consisted of significant bending and was bound of bending losses. In 2016, *Yang Wang* et al proposed a 3 dB splitter design with adiabatic tapered silicon waveguide [11]. A 3 dB power splitting is achieved by introducing a bending to facilitate the separation for inhibiting the re-coupling of the optical power. The author of this manuscript has adopted the same methodology of intra-modal coupling between waveguides for splitting, but with a different design structure. In 2018, another team of *Yesica Bustamante et. al.* proposed a 3 dB tapered splitter design [28]. The author utilized the bending for the separation of two secondary waveguides to restrict the re-coupling of the optical split power. The design incorporated an insertion loss of 0.5 dB and 0.07 dB for TE and TM polarization modes.

In all the above-mentioned manuscripts, the adopted principle for 3 dB splitting is similar, but the distinctiveness of this research is to split light in the secondary waveguide by inhibiting re-coupling, thereby getting equal power at the output ports.

2 Design and Theory

Section of this paper discusses the proposed design for 3-dB splitter and builds a theoretical model of transfer of normalized power, in direction of the propagation of wave, between primary and secondary waveguide. For ease of mathematics, the theoretical model considers only one set of primary-secondary waveguides. Although, the model is applicable on both the set of the waveguides with unchanged behavior.

The proposed design consists of three-cuboidal waveguides with rectangular cross-section. For ease of explanation, the central waveguide is named as primary waveguide while other two as secondary waveguide. Primary and secondary waveguides are fabricated inside a substrate of silica glass (SiO_2). Both the waveguides are composed of undoped pure silicon. Silicon is taken as the fabrication material because of high contrast of refractive indices between silica glass substrate and silicon in both primary and secondary waveguides. In addition to this, the high abundance of silicon in nature is also a qualifying factor.

The structure is symmetric about the y-z, x-z and x-y plane and is assumed to be non-varying along the longitudinal length. All the intrinsic losses are ignored and only coupling loss is considered for the design. A 3-D view of the design is shown in Fig. 1.

Width of the rectangular cross-section of primary and secondary waveguides is taken as $w_r = 400\ nm$ and the height of cross-section of the waveguides are taken as standard fabrication value $h_r = 220\ nm$. The width of the cross-section has been optimized, which is discussed in

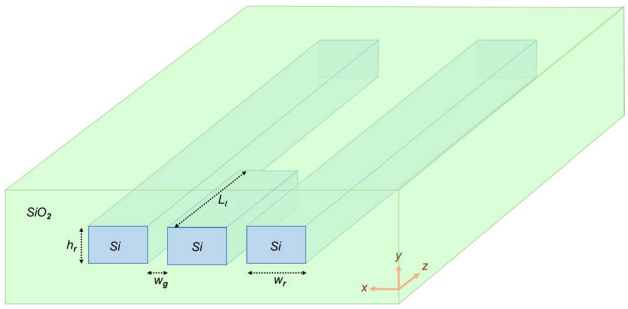

Fig. 1 3-D view for the schematic structure of 3-dB splitter

further sections of the paper. The gap between both the waveguides is an important parameter of the design. It plays a significant role in the intra-waveguide modal coupling, in which higher gap owes to reduced modal coupling. Thus, it is mandatory to get an optimized value of the gap. This gap too is optimized and is discussed in detail in further sections of the paper. For this design, the gap is taken as $w_g = 55\ nm$. Refractive index of silica glass and silicon are evaluated using Sellmeier Equation [29, 30].

Flourishing research in nano optical devices lead to fast and accurate numerical tools. Finite Element Method (FEM) and Finite-Difference Time-Domain (FDTD) are the two well-known methods for which simulators are available nowadays for the design of optical devices. The shrinking size of optical devices have brought intense computational burden for simulation and result accuracy. Therefore, the need for high computational performance is shooting up [31]. Due to the difference of numerical algorithms between FDTD and FEM, FEM performs better than FDTD for nano optical devices. The time iteration of FEM to achieve numerical stability and accuracy are less in comparison to FDTD. Therefore, FEM is employed for the computation of differential equations by meshing the cross-section and dividing the area into sub-domains.

An EM wave travels in a waveguide with a propagation constant 'β' and supports several guided modes, defined by the boundary condition and the structure. Let's take a case where a primary and one secondary waveguide are fabricated next to each other as shown in Fig. 2. The EM wave travels in the primary and secondary waveguide with a propagation constant of β_a and β_b, assuming $\beta_a < \beta_b$, and their respective modal field distribution be ψ_a and ψ_b. When the gap between primary and secondary waveguide is large enough, the EM wave propagates with their respective propagation constant, i.e., β_a and β_b and there is no influence of normal modes onto each other. However, as the gap is reduced, the canonical modal fields of the waveguides suffer modification due to the interaction between the canonical normal modes. This interaction originates due to the evanescent fields of the primary and secondary waveguide. Due to the modification, canonical modes vanish and two new modes originate, ψ_e (even mode) and ψ_o (odd mode) which propagate along the longitudinal length of the waveguide with their respective propagation constants β_e and β_o, where $\beta_e > \beta_o$. When an even and odd mode is excited simultaneously, the modes travel at different speeds due to varying propagation constant values. This results in beating phenomena due to which the power is transferred from one mode to another periodically along the longitudinal length [12].

The intention is to build a mathematical model of normalized power flux along the waveguide and the exchange of power between the primary and secondary waveguides. For the same purpose, two modes ('a' and 'b') are considered. Using the coupling modal equation, Eqs. 1 and 2 [32].

$$\frac{dA(z)}{dz} = -ik_{ab}B(z)e^{-i(\beta_b-\beta_a)z} \tag{1}$$

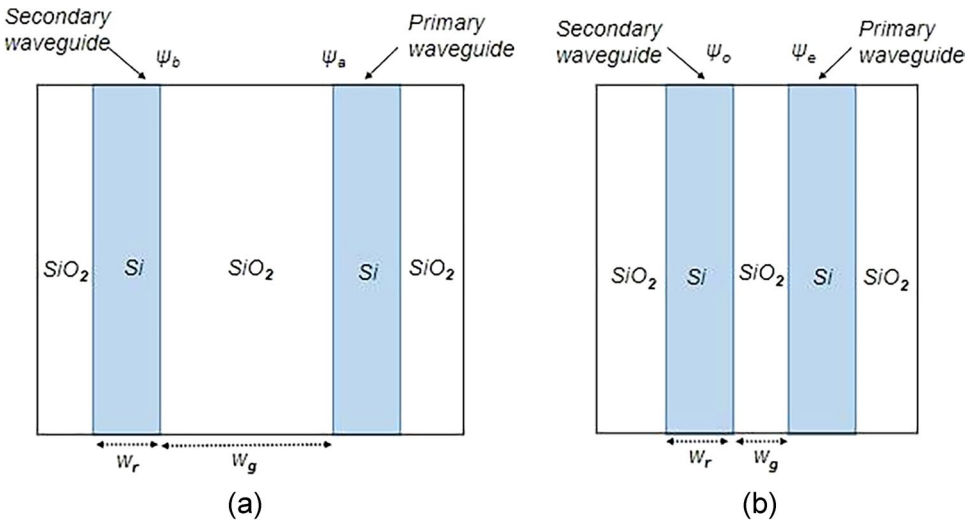

Fig. 2 Primary and secondary waveguide with (**a**) No coupling; and (**b**) Mutual coupling

$$\frac{dB(z)}{dz} = -ik_{ba}A(z)e^{-i(\beta_b-\beta_a)z} \tag{2}$$

Where, A(z) and B(z) denote the expansion coefficient of mode '*a*' and mode '*b*' with z-axis as the propagation direction of the electromagnetic field. Expansion coefficient represents the contribution of the mode in total EM wave. K_{ab} and K_{ba} denotes coupling coefficients between two modes. Since, it has been assumed that the waveguides are non-absorbing, it is fair to say $k_{ab} = k_{ba} = k$. Thus Eqs. 1 and 2 is re-written as

$$\frac{dA(z)}{dz} = -ikB(z)e^{-i(\beta_b-\beta_a)z} \tag{3}$$

$$\frac{dB(z)}{dz} = -ikA(z)e^{-i(\beta_b-\beta_a)z} \tag{4}$$

Equations 3 & 4 are differential equations with respect to z. To solve the differential equation, it is assumed that

$$A(z) = Ae^{-i\gamma z}e^{-i\Delta Z} \tag{5}$$

$$B(z) = Be^{-i\gamma z}e^{+i\Delta Z} \tag{6}$$

In the assumed solution two new parameters: Δ and γ are introduced, as shown in Eq. 7 Δ indicates the level of modal phase matching and is helpful in finding the condition for efficient coupling between the waveguides. Δ = 0 indicates the perfect matching of modes and thus there will be the most efficient coupling between the waveguides.

$$\Delta = \frac{\beta_b - \beta_a}{2} \text{ and } \gamma = \pm\sqrt{k^2 + \Delta^2} \tag{7}$$

From Eqs. 5 and 6, the ratio of the constants 'B' and 'A' can be written as

$$\frac{B}{A} = \frac{k}{(\gamma - \Delta)} \tag{8}$$

Now, considering both the signs of γ, the solution of A(z) and B(z) becomes

$$A(z) = \left(A_e e^{-i\gamma z} + A_o e^{i\gamma z}\right)e^{-i\Delta z} \tag{9}$$

$$B(z) = \left(\frac{A_e k}{\gamma - \Delta}e^{-i\gamma z} + \frac{A_o k}{\gamma + \Delta}\right)e^{-i\Delta Z} \tag{10}$$

A_e and A_o correspond to respective constants for even and odd modes after considering the positive and negative sign over γ. The initial condition for the system is taken as A(0) = 1 and B(0) = 0, with an assumption that power is injected in only the primary waveguide, at z = 0. Putting the condition in Eqs. 9 and 10 and solving the simultaneous equations, the constants A_e and A_o can be evaluated.

$$A_e + A_o = 1 \tag{11}$$

$$\frac{A_e k}{\gamma - \Delta} - \frac{A_o k}{\gamma + \Delta} = 0 \tag{12}$$

Once A_e and A_o are evaluated, their values are replaced in Eqs. 9 and 10 and the equation becomes-

$$A(z) = \left\{\cos(\gamma z) + i\frac{\Delta}{\gamma}\sin(\gamma z)e^{-i\Delta Z}\right\} \tag{13}$$

$$B(z) = -i\frac{k}{\gamma}\sin(\gamma z)e^{-i\Delta Z} \tag{14}$$

The power flux along the primary and secondary waveguide can be calculated by squaring the expansion coefficients [12]. Thus, normalized power flux along secondary waveguide is given by-

$$\frac{|B(z)|^2}{|A(0)|^2} = \left(\frac{k}{\gamma}\right)^2 \sin^2(\gamma z) \tag{15}$$

Considering the case of perfect matching, where Δ = 0, γ = *k*. Thus, Eq. 15 becomes

$$\frac{|B(z)|^2}{|A(0)|^2} = \sin^2(\gamma z) \tag{16}$$

Maximum value for normalized power flux in secondary waveguide is attained when γz = π/2. That is, as the mode travels π/2γ unit longitudinally, the entire power injected into the primary waveguide is transferred to the secondary waveguide. This length is known as coupling length and is denoted by L_c. Thus, Eq. 16 can be reframed as-

$$\frac{|B(z)|^2}{|A(0)|^2} = \sin^2\left(\frac{\pi}{2L_c}z\right) \tag{17}$$

Similarly, power flux along the primary waveguide can be evaluated by squaring the expansion coefficient B(z). Therefore, normalized power flux along the primary waveguide is given by-

$$\frac{|A(z)|^2}{|A(0)|^2} = \left(\frac{\Delta}{\gamma}\right)^2 + \left(1 - \left(\frac{\Delta}{\gamma}\right)^2\right)\cos^2\left(\frac{\pi}{2L_c}z\right) \tag{18}$$

For matched modes, Δ = 0 and Eq. 18 shorten to-

$$\frac{|A(z)|^2}{|A(0)|^2} = \cos^2\left(\frac{\pi}{2L_c}z\right) \tag{19}$$

Equations 17 and 19 shows the normalized power flux along secondary and primary waveguide in phase matching condition respectively. As evident, there is a back-and-forth transfer of power between both the waveguides.

3 Cross-Sectional Width Optimization of Waveguide

The width of a rectangular cross-sectional cuboidal waveguide is an important dimensional parameter for the confinement of the EM wave inside the waveguide. This section of paper discusses width (w_r) optimization of primary and secondary waveguide. The qualification factor for the optimization is taken as confinement factor and mode effective area. Figure 3 shows a single rectangular cross-sectional waveguide-.

An analysis is made by sweeping the value of w_r from *50 nm* to *1000 nm* and studying the trends of confinement factor and mode effective area with respect to w_r. The reason behind choosing this sweep range is to find out the optimized value of the w_r that yields the propagation of maximum power flux in the cross-section of the primary and secondary waveguides. In Fig. 4, the analysis suggests that as the width increases, the confinement factor initially increases and then saturates to ~75%. Confinement factor is a parameter that tells the level of mode confinement inside the cross-section of the waveguide. The graph suggests that at $w_r = 400\ nm$, the confinement factor in the cross-section starts saturating. The proposed design is constructed in such a way that it supports a single mode due to which the confinement factor gets saturated on increasing the width of the waveguide (w_r).

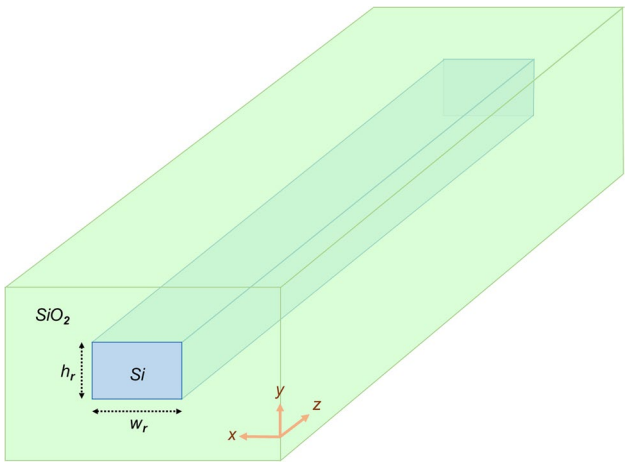

Fig. 3 3D schematic view of cuboidal waveguide with rectangular cross-section

In contrast, as width increases, the mode effective area decreases steeply as shown in Fig. 5. Mode effective area explain the density of the modes in the cross-section of the waveguide. The graph is exponentially decreasing in nature which grazes the axis from $w_r = 200\ nm$.

To find the optimized value of the width, an intersection of results of confinement factor and mode effective area is considered. Based on this, $w_r = 400\ nm$ is concluded to be the optimized width for the primary and secondary waveguides.

4 Gap Optimization of between Waveguides

The optimized w_r ensure an efficient confinement of EM waves and a very less mode effective area. Next concern is the gap (w_g) parameter between primary and secondary waveguides. As w_g increases, the evanescent field in primary and secondary waveguide fails to interact with each other, resulting in reduced modal coupling and further

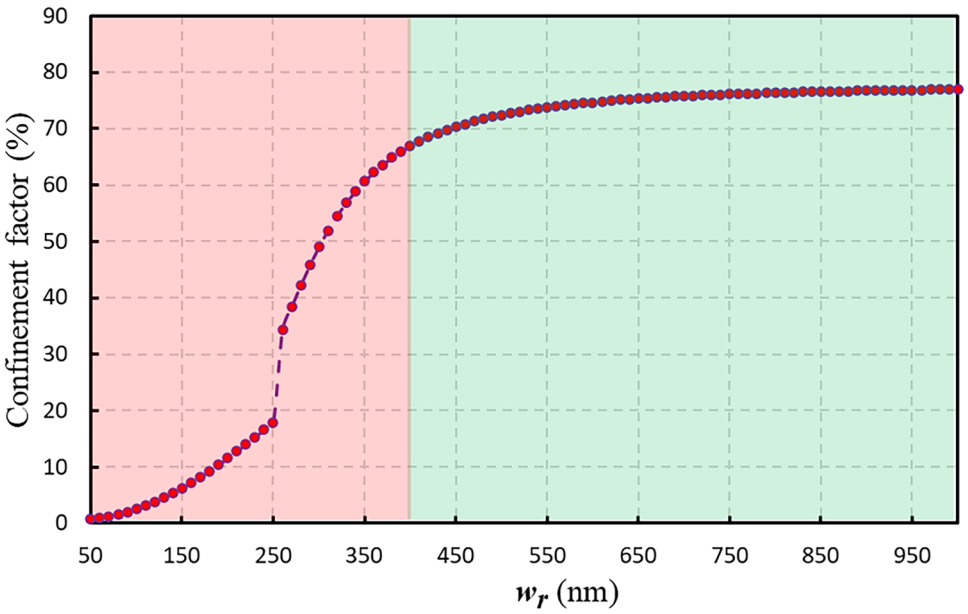

Fig. 4 Confinement loss with respect to different w_r

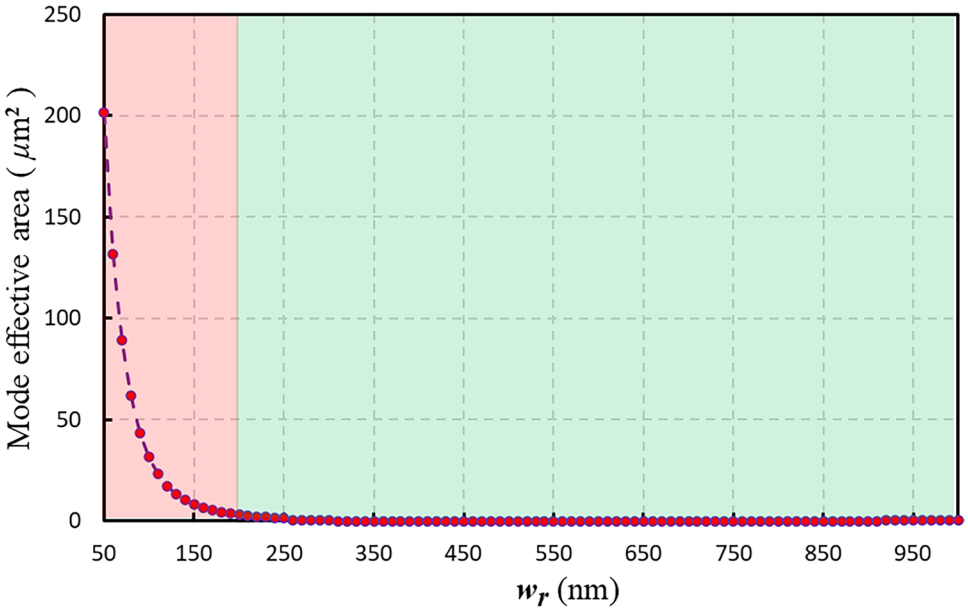

Fig. 5 Mode effective area with respect to different w_r

zero mode coupling. Due to this, the modes are unable to exchange power with each other and the fundamental principle of the 3-dB splitter fails to satisfy. Therefore, it is mandatory to find an optimized value of the gap.

An analysis has been made in which the value of the gap is swept from *0 nm* to *200 nm* and normalized volume intensity is evaluated corresponding to the w_g values. For the analysis, only one set of primary and secondary waveguides is considered. However, the results are applicable on both. The variation in normalized volume intensity is shown in Fig. 6.

The graph in Fig. 6 suggests that when w_g is less than *55 nm,* there is an arbitrary exchange of power between the two waveguides. As $w_g > 55$ *nm,* the volume intensity in the secondary waveguide decreases. This infers that the coupled power in the secondary waveguide is reduced due to reduced modal coupling. Similarly, for $w_g > 55$ *nm,* volume intensity in primary waveguide is increasing which in return infers that the modal power is sustained in the waveguide and power is not being coupled to the secondary waveguide. Based on this result, it is concluded that, $w_g = 55$ *nm* is the optimized value of the w_g between two waveguides.

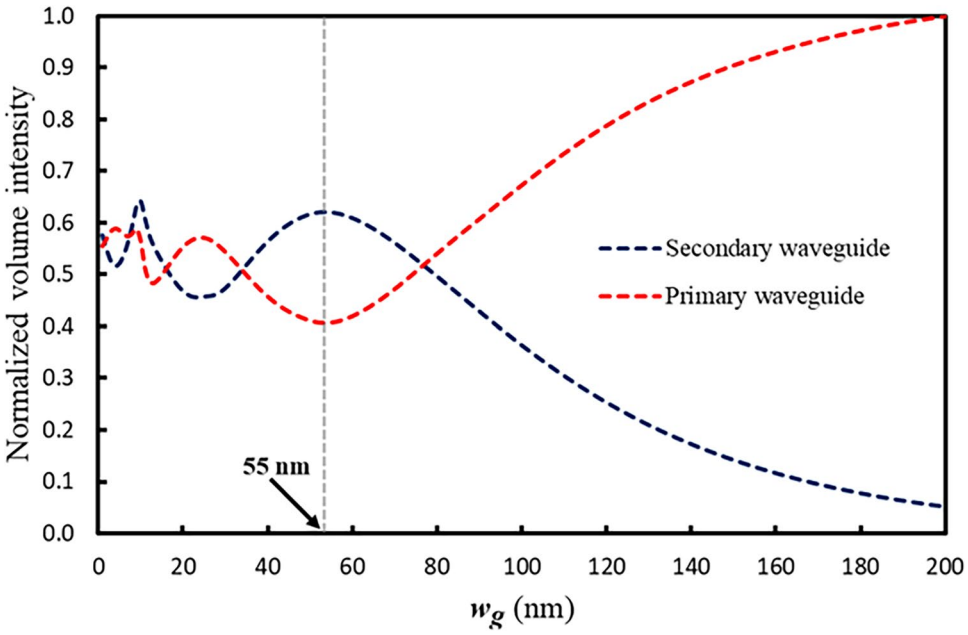

Fig. 6 Normalized volume intensity in primary and a secondary waveguide with respect to w_g

5 Longitudinal Length Optimization of Primary Waveguide

In this section of the paper, the optimum longitudinal length (L_l) of the primary waveguide is calculated. Intention behind finding the optimum length is to provide a structure that inhibits the coupling between primary and secondary waveguide at a point where all the power flux has been transferred to the secondary waveguide. For calculation purposes, three-cuboidal waveguides of the same length are considered initially, as shown in Fig. 7. The power flux exchange between primary and secondary waveguide is observed. Based on the results of power distribution, the optimum length is decided.

Figure 8 shows the power flux distribution between primary and secondary waveguides. The exchange of power flux is periodical along the longitudinal length. The power flux injected in the primary waveguide is split into two secondary waveguides uniformly after a definite length. This split power in secondary waveguides, further couples back to the primary waveguide to return the injected power to the primary waveguide. Thus, there is an exchange of power flux in repetition along the entire propagation length of the waveguides.

It is observed from Fig. 8 that there is a finite longitudinal length of primary waveguide, at which the entire injected power from primary waveguide is transferred, for the first time, to secondary waveguides and no more net power flux is remaining in the primary waveguide. This longitudinal length is of concern to the design of 3 dB splitter. The proposed splitter design supports TE mode of propagation only. Thus, TM mode of propagation is not supported by the design.

The power flux relation with propagational length is visualized for primary and secondary waveguides individually by drawing cut-lines through the center of waveguide. These cut lines are helpful in computing the poynting vector along the direction of propagation (z-direction) of the

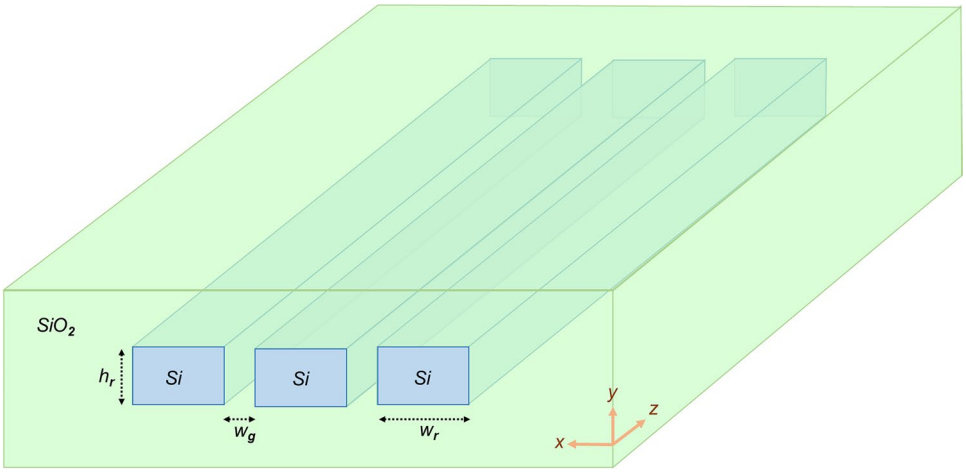

Fig. 7 3D view of Equi-longitudinal length primary and secondary waveguides

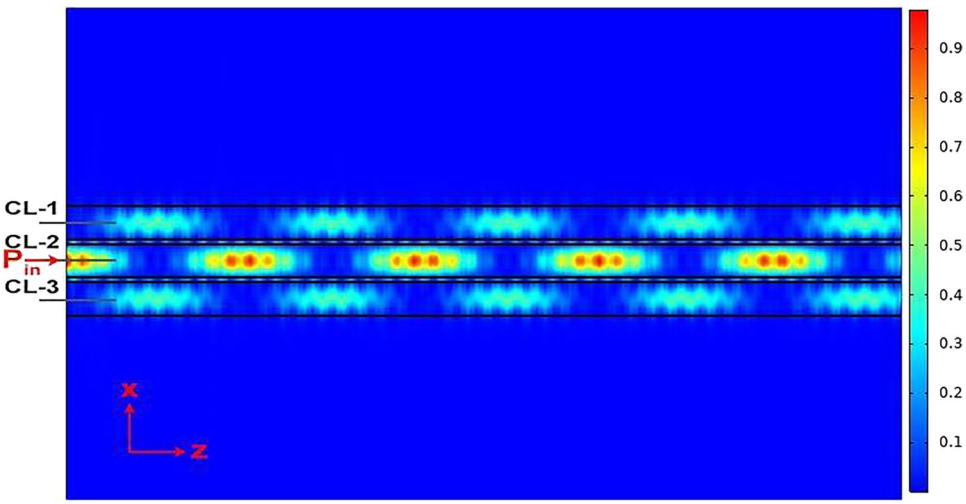

Fig. 8 Top view of power flux distribution between primary and secondary waveguide

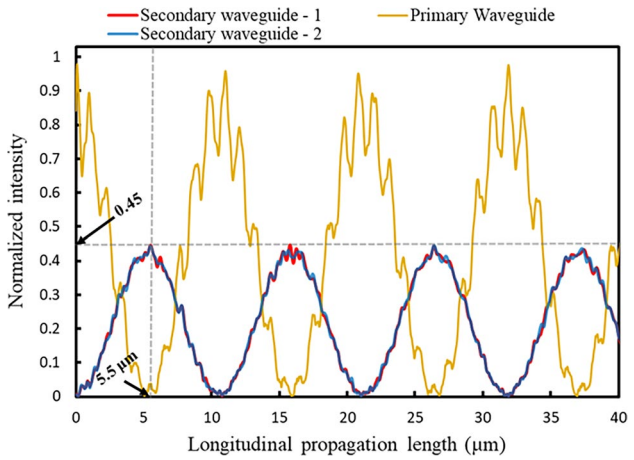

Fig. 9 Relation of normalized power flux in primary and secondary waveguide with respect to longitudinal length

waveguides. The power flux relation with propagation length is shown in Fig. 9 for each waveguide respectively.

As shown in Fig. 9, the normalized power flux in primary and secondary waveguide, with respect to longitudinal length, is a sinusoidal graph. This graph justifies the theoretical model that is formulated in section-2 of the paper. In Eq. (17) and (19), normalized power flux in primary and secondary waveguides is sinusoidal in nature. Precisely, normalized flux in primary waveguide is a cosine of z and L_c whereas normalized power flux in secondary waveguide is a sine in z and L_c. This relation is justified in Fig. 9 where the plotted graph of normalized intensity in primary and secondary waveguides is 90° out of phase to each other and is sinusoidal in nature.

Graph in Fig. 9 suggests that at $z = 5.5\ \mu m$, power flux in the primary waveguide is approximately vanished and this power is transferred to the secondary waveguides in equal proportion. Normalized flux in the secondary waveguide, at $z = 5.5\ \mu m$, is nearly *~0.45 or 45%.*

By stopping intra-modal coupling at this point, power flux exchange can be stopped thereby constraining 50%–50% power in both secondary waveguides. As the power flux is injected in the primary waveguide, it splits equally into secondary waveguides at a finite distance in the primary waveguide. This L_l of the primary waveguide has been chosen intentionally in such a way that the split power in respective secondary waveguides cannot re-couple into the primary waveguide. Thus, precise selection of L_l of the primary waveguide leads to the inhibition of intra-modal coupling between primary and secondary waveguides. Conclusively, $L_l = 5.5\ \mu m$ is the best possible value of longitudinal length for primary waveguide. The evaluated coupling length is for TE mode of propagation.

6 Results and Discussion

In the last section, the optimum value of L_l is evaluated and is taken as *5.5 μm.* Input power of *10 mW* is injected at the port of the primary waveguide of design shown in Fig. 1. For analysis purposes, three ports at the other rectangular cross-sectional end of the waveguides are defined. A cut-line is drawn, connecting both ends of the waveguides, along the longitudinal length of all the cuboidal waveguides for study of power flux. Figure 10 shows the top view of power flux distribution in the proposed design.

It is clearly visible from the Fig. 10 that the injected power from the primary waveguide is uniformly split into two secondary waveguides. Thereafter, due to the short length of the primary waveguide, there is no exchange of power flux after $z = 5.5\ \mu m$ and power is unable to recollect back to the primary waveguide. Moreover, by

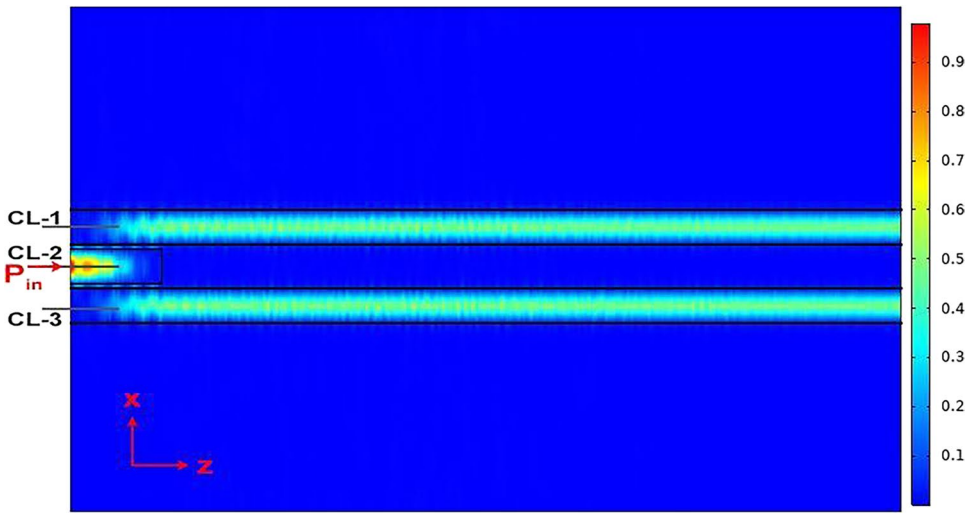

Fig. 10 Top view of power flux distribution in primary and secondary waveguide with $L_l = 5.5\ \mu m$

analysis of Fig. 6, it is known that when the gap between two waveguides is more than *55 nm,* there is no intra-modal coupling. Due to this, there is no modal coupling between two secondary waveguides, as the gap between two secondary waveguides is *510 nm*.

Figure 11 shows the graphical relation of normalized power flux with respect to the longitudinal length of the cuboidal waveguides. As evident from the Fig. 11, normalized power flux in secondary waveguides increases till $z = 5.5\ \mu m$ where z denotes the propagation length variable. As $z > 5.5\ \mu m$, power flux across the secondary waveguides become constant to 0.45 or 45% of the injected power. Throughout the length of the waveguides, normalized power remains approximately the same. Similarly, power flux in primary waveguide reduces till $z = 5.5\ \mu m$ and further vanishes.

The fabrication errors and variations play an important role in deciding the efficiency and behavior of the design after fabrication of the SoI system. Simulation is performed by changing the w_r and w_g of the waveguide by ±5% of optimized parameter. This analysis is known as fabrication tolerance analysis and shown in Fig. 12. The result infers that there is not a significant impact of geometrical variations in the output power flux from primary and secondary ports for the proposed design.

The design works on the principle of intra-modal coupling due to the presence of evanescent fields in respective primary and secondary waveguides. The loss associated with this 3 dB splitter is excess loss, which is related to input and output power of primary and secondary arm of the waveguide [33]. The proposed design accounts for an average of $-0.05\ dB$ of excess loss for C-band wavelengths as shown in Fig. 13. Thus, this excess loss is responsible for a 45%–45% split power ratio in secondary waveguides.

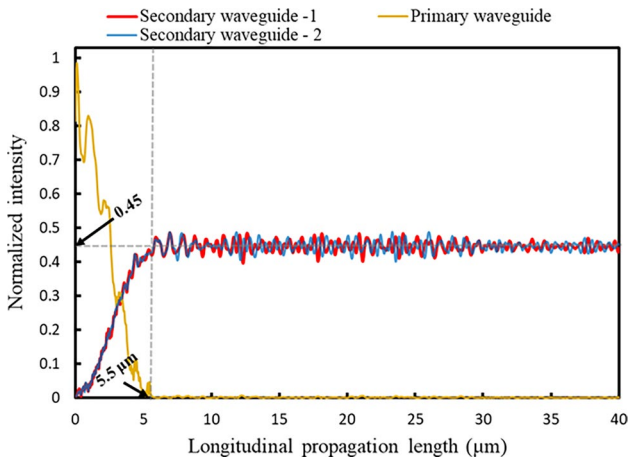

Fig. 11 Relation of normalized power flux in primary and secondary waveguide with respect to longitudinal length with $L_l = 5.5\ \mu m$

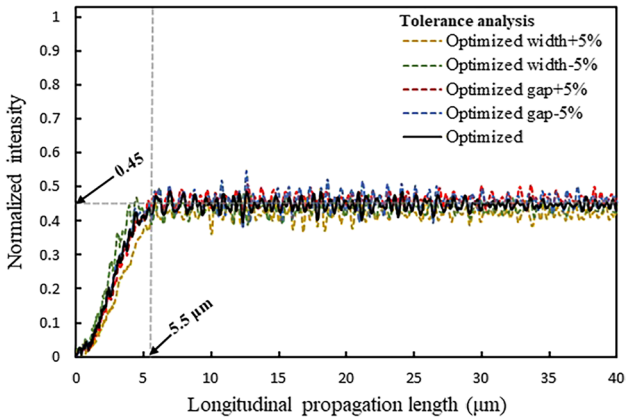

Fig. 12 Fabrication tolerance analysis by varying ± 5% in w_r and w_g of the waveguide

In addition to this, the proposed design is independent of the wavelength of input optical light. It is confirmed in Fig. 13 that the behavior of the splitter remains the same for all the wavelengths. For an entire C-band of 35 nm (1530 nm to 1565 nm), the normalized transmittance is nearly ~0.46.

At last, it is important to discuss the comparison of the proposed design with the other publications. In 2013, *Zhe Xiao* et al proposed a wavelength-independent, polarization insensitive and low loss 3 dB Y-Junction waveguide based power splitter [34]. In that design, an excess loss of $-0.11\ dB$ and $-0.18\ dB$ was associated for TE and TM mode. In 2016, *Hongnan Xu* et al utilized a Y junction waveguide for creating an ultra-broadband dual-mode 3 dB power splitter [35]. The proposed design yielded an excess loss of *0.45 dB* and *0.5 dB* for TM_0 and TM_1 mode respectively. The design consisted of a Y shaped waveguide which had a slight bending to produce separation between adjacent waveguides such that the split light can be inhibited from re-coupling. In 2016, *Yang Wang* et al proposed ultra-broadband and low-loss

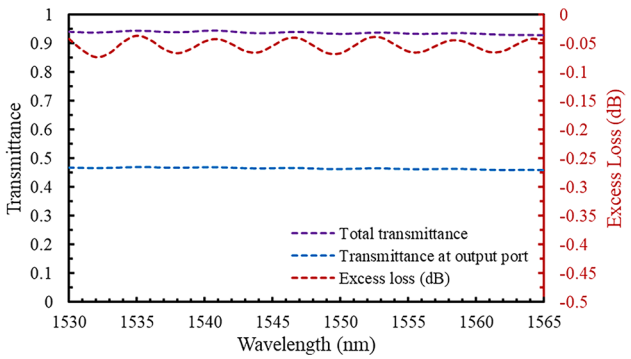

Fig. 13 Transmittance and excess loss with respect to C-band of wavelengths (1530 nm–1565 nm)

3 dB power splitter design based on adiabatic silicon waveguide [11]. The design involved bending as well as tapering to provide the separation for the application of power splitting in respective secondary waveguides. The design showcased an excess loss of less than *0.19 dB* for TE and *0.14 dB* for TM mode respectively. In 2019, *Chonglei Sun* et al came up with another splitter design with multi-mode tapered branches [36]. This design also consist of Y branch junction and bendings.

The proposed design utilizes only three straight rectangular waveguides arranged parallel to each other with optimized w_g of 55 nm. This design consist of one primary waveguide of optimized propagation length of *5.5 μm*. There is no bending and tapering in this 3 dB power splitter. Also an average excess loss of *−0.05 dB* is witnessed for the C-band wavelengths in TE mode, which is very less in comparison to mentioned publication in comparison.

7 Conclusion

The paper presents a SoI based 3 dB power splitter design in which three-cuboidal waveguides with rectangular cross-sectional area are brought into use. Power of *10 mW* is injected at the port of the primary waveguide. This power further gets split nearly into equal halves in secondary waveguides, thereby providing a 3 dB split power at the output ports of secondary waveguides. Nearly 45% - 45% of total power is transferred to both the secondary waveguides. In addition to this, in case of $z > L_l$, power flux remains the same throughout the length of the secondary waveguides and thus power flux in the secondary waveguide does not depend on the longitudinal length of the secondary waveguide. This design involves no tampering or bending of the cuboidal waveguides. Due to this, there is no scope of bending loss involved in the design. This reduces the losses associated with the splitter design. Also, the design is insensitive and independent of the wavelength of input power.

Acknowledgements This work has been carried out in Netaji Subhas University of Technology, Delhi.

Author Contributions Devansh Srivastava and Shalini Vardhan: Performed simulations, Data collection, Data curation, Writing - Original draft. Ritu Raj Singh: Conceptualization, Review and Editing.

Data Availability The datasets generated during and/or analyzed during the current study are available from the corresponding author on reasonable request.

Declarations

This research do not involve any Human Participants and/or Animals.

Ethics Approval The authors ensure that accepted principles of ethical and professional conduct have been followed during this research work.

Consent to Participate Consent was obtained from all the authors contributed in the research work.

Consent for Publication The authors give full consent for publication of this research work.

Conflict of Interest The authors declare no conflicts of interest.

References

1. Snyder AW, Love JD (1984) Optical waveguide theory. Springer US, Boston, MA. https://doi.org/10.1007/978-1-4613-2813-1
2. Tomofuji S, Matsuo S, Kakitsuka T, Kitayama K (2009) Dynamic switching characteristics of InGaAsP/InP multimode interference optical waveguide switch. Opt Express 17(26):23380. https://doi.org/10.1364/OE.17.023380
3. Jalalifar M, Uddin MJ (2011) Power splitter architectures and applications. Progress In Electromagnetics Research C 18:231–244. https://doi.org/10.2528/PIERC10101004
4. Li T et al (2013) Low-voltage, high speed, compact silicon modulator for BPSK modulation. Opt Express 21(20):23410. https://doi.org/10.1364/OE.21.023410
5. Chen S, Shi Y, He S, Dai D (2015) Compact monolithically-integrated hybrid (de)multiplexer based on silicon-on-insulator nanowires for PDM-WDM systems. Opt Express 23(10):12840. https://doi.org/10.1364/OE.23.012840
6. Han L, Kuo BP-P, Alic N, Radic S (2018) Ultra-broadband multimode 3dB optical power splitter using an adiabatic coupler and a Y-branch. Opt Express 26(11):14800. https://doi.org/10.1364/OE.26.014800
7. Mohammadi M, Olyaee S, Seifouri M (2019) Passive integrated optical gyroscope based on photonic crystal ring resonator for angular velocity sensing. Silicon 11(6):2531–2538. https://doi.org/10.1007/s12633-018-0040-9
8. Mohammadi M, Fallahi V, Seifouri M (2021) Optimization and performance analysis of all-optical compact 4 and 5-channel Demultiplexers based on 2D PC ring resonators for applications in advanced optical communication systems. Silicon 13(8):2619–2629. https://doi.org/10.1007/s12633-020-00614-y
9. Tan Q, Huang X, Zhou W, Yang K (2013) A Plasmonic based Ultracompact polarization beam splitter on silicon-on-insulator waveguides. Sci Rep 3(1):2206. https://doi.org/10.1038/srep02206
10. Li H et al (2020) Compact and low-loss 1 × 3 polarization-insensitive optical power splitter using cascaded tapered silicon waveguides. Opt Lett 45(19):5596. https://doi.org/10.1364/OL.401036
11. Wang Y, Gao S, Wang K, Skafidas E (2016) Ultra-broadband and low-loss 3 dB optical power splitter based on adiabatic tapered silicon waveguides. Opt Lett 41(9):2053. https://doi.org/10.1364/OL.41.002053
12. Radhakrishnan S, Kumar DS, Raja GT (2021) Design and simulation analysis on TM–pass GST-assisted asymmetric directional coupler-based polarizer. Silicon. https://doi.org/10.1007/s12633-021-01406-8
13. Xiao J, Guo Z (2018) Ultracompact polarization-insensitive power splitter using subwavelength gratings. IEEE Photon Technol Lett 30(6):529–532. https://doi.org/10.1109/LPT.2018.2801337
14. Yang H, Kuan Y, Xiang T, Zhu Y, Cai X, Liu L (2018) Broadband polarization-insensitive optical switch on silicon-on-insulator platform. Opt Express 26(11):14340. https://doi.org/10.1364/OE.26.014340

15. Gao S et al (2019) Fast polarization-insensitive optical switch based on hybrid silicon and Lithium Niobate platform. IEEE Photon Technol Lett 31(22):1838–1841. https://doi.org/10.1109/LPT.2019.2949090
16. Zhang J-X (2022) Design of broadband and compact mid-infrared polarization beam splitter based on all-circular air holes with low loss. J Nanophoton 16(1):016005. https://doi.org/10.1117/1.JNP.16.016005
17. Lagali NS, Paiam MR, MacDonald RI, Worhoff K, Driessen A (1999) Analysis of generalized Mach-Zehnder interferometers for variable-ratio power splitting and optimized switching. J Light Technol 17(12):2542–2550. https://doi.org/10.1109/50.809675
18. Wei H, Yu J, Zhang X, Liu Z (2001) Compact 3-dB tapered multimode interference coupler in silicon-on-insulator. Opt Lett 26(12):878. https://doi.org/10.1364/OL.26.000878
19. Dai D, He S (2006) Optimization of Ultracompact polarization-insensitive multimode interference couplers based on Si nanowire waveguides. IEEE Photon Technol Lett 18(19):2017–2019. https://doi.org/10.1109/LPT.2006.882227
20. Wei H, Jinzhong Y, Liu Z, Zhang X, Shi W, Fang C (2001) Fabrication of 4 x 4 tapered MMI coupler with large cross section. IEEE Photon Technol Lett 13(5):466–468. https://doi.org/10.1109/68.920753
21. Frandsen LH et al (2004) Ultralow-loss 3-dB photonic crystal waveguide splitter. Opt Lett 29(14):1623. https://doi.org/10.1364/OL.29.001623
22. Nguyen VH, Kim IK, Seok TJ (2020) Low-loss and broadband silicon photonic 3-dB power splitter with enhanced coupling of shallow-etched rib waveguides. Appl Sci 10(13):4507. https://doi.org/10.3390/app10134507
23. Kim S, Park I, Lim H (2005) Proposal for ideal 3-dB splitters–combiners in photonic crystals. Opt Lett 30(3):257. https://doi.org/10.1364/OL.30.000257
24. Tao S, Yang B, Xia H, Wang H, Lo G-Q (2011) An optical power splitter with variable power splitting ratio. IEEE Photon Technol Lett 23(14):1004–1006. https://doi.org/10.1109/LPT.2011.2150209
25. Chen X, Liu W, Zhang Y, Shi Y (2017) Polarization-insensitive broadband 2 × 2 3 dB power splitter based on silicon-bent directional couplers. Opt Lett 42(19):3738. https://doi.org/10.1364/OL.42.003738
26. Yun H, Shi W, Wang Y, Chrostowski L, Jaeger NAF (2013) 2×2 adiabatic 3-dB coupler on silicon-on-insulator rib waveguides. 89150V. https://doi.org/10.1117/12.2037968
27. Wang H-T, Chen C-F, Chi S (2015) A good performance 3-dB splitter based on coupling-weighted and velocity-tapered waveguides. Opt Commun 350:97–102. https://doi.org/10.1016/j.optcom.2015.03.055
28. Bustamante Y, Farias G (2018) Demonstration of broadband and polarization-insensitive silicon photonics 3 dB splitter compatible with CMOS process, in 2018 SBFoton International Optics and Photonics Conference (SBFoton IOPC), 1–4. https://doi.org/10.1109/SBFoton-IOPC.2018.8610944
29. Singh RR, Srivastava D, Bhattacharya W (2021) Analysis of solid-core photonic crystal Fiber for confinement loss and birefringence with square air hole layers. in Frontiers in Optics + Laser Science 2021,JTh5A.64. https://doi.org/10.1364/FIO.2021.JTh5A.64
30. Singh RR (2020) Dispersion tailoring of silicon nanowire optical rectangular waveguide (SNORW). SN Appl Sci 2(3):502. https://doi.org/10.1007/s42452-020-2309-z
31. Liu Y-C, Chang K, Fwu J, Shih L (2013) Performance comparison between FDTD and FEM for the simulation of plasmonic waveguide operating at optical communication frequency, in 2013 USNC-URSI Radio Science Meeting (Joint with AP-S Symposium), 184–184. https://doi.org/10.1109/USNC-URSI.2013.6715490
32. Lifante G (2004) Integrated Photonics, 90
33. Purnamaningsih RW, Poespawati NR, Dogheche E (2019) Design of a Four-Branch Optical Power Splitter Based on gallium-nitride using rectangular waveguide coupling for telecommunication links. J Eng 2019:1–9. https://doi.org/10.1155/2019/7285305
34. Xiao Z et al (2013) Ultra-compact low loss polarization insensitive silicon waveguide splitter. Opt Express 21(14):16331. https://doi.org/10.1364/OE.21.016331
35. Xu H, Shi Y (2016) Ultra-broadband dual-mode 3 dB power splitter based on a Y-junction assisted with mode converters. Opt Lett 41(21):5047. https://doi.org/10.1364/OL.41.005047
36. Sun C, Zhao J, Wang Z, Du L, Huang W (2019) Broadband and high uniformity Y junction optical beam splitter with multimode tapered branch. Optik (Stuttg) 180:866–872. https://doi.org/10.1016/j.ijleo.2018.12.013